Nuclear matter distributions in the neutron-rich carbon isotopes $^{14-17}$C from intermediate-energy proton elastic scattering in inverse kinematics

A.V. Dobrovolsky[a,*], G.A. Korolev[a], S. Tang[b,1], G.D. Alkhazov[a], G. Colò[c], I. Dillmann[b], P. Egelhof[b], A. Estradé[b,2], F. Farinon[b], H. Geissel[b], S. Ilieva[b], A.G. Inglessi[a], Y. Ke[b,1], A.V. Khanzadeev[a], O.A. Kiselev[b], J. Kurcewicz[b,3], X.C. Le[b], Yu.A. Litvinov[b], G.E. Petrov[a], A. Prochazka[b], C. Scheidenberger[b], L.O. Sergeev[a], H. Simon[b], M. Takechi[b,4], V. Volkov[b,5], A.A. Vorobyov[a], H. Weick[b], V.I. Yatsoura[a]

[a] *Petersburg Nuclear Physics Institute, National Research Centre Kurchatov Institute, Gatchina, 188300 Russia*
[b] *GSI Helmholtzzentrum für Schwerionenforschung GmbH, 64291 Darmstadt, Germany*
[c] *Dipartimento di Fisica, Università degli Studi di Milano and INFN, Sezione di Milano, Via Celoria 16, 20133 Milano, Italy*

Abstract

The absolute differential cross sections for small-angle proton elastic scattering off the nuclei $^{12,14-17}$C have been measured in inverse kinematics at energies near 700 MeV/u at GSI Darmstadt. The hydrogen-filled ionization chamber IKAR was used as an active target to detect the recoil protons. The measured cross sections were analysed using the Glauber multiple-scattering theory. The radial nuclear matter density distributions and the root-mean-square nuclear matter radii were obtained. A possible neutron halo structure in ^{15}C, ^{16}C and ^{17}C is discussed. The obtained data show evidence for a halo structure in the ^{15}C nucleus.

Keywords: ^{12}C, ^{14}C, ^{15}C, ^{16}C, ^{17}C, nuclear matter distribution, nuclear matter radii, proton-nucleus elastic scattering

1. Introduction

The study of nuclei far from stability is a topic of great current interest. A number of experiments have shown that these nuclei may have exotic structures such as a neutron skin or a halo [1–4]. The neutron skin describes an excess of neutrons on the nuclear surface whereas the halo corresponds to such an excess along with an extended tail of the neutron density distribution. The necessary conditions for the halo formation in nuclei are a small binding energy and a low angular momentum of the valence nucleon(s). It has been found that a halo structure manifests itself by large interaction (reaction) cross sections, by enhanced removal cross sections and by narrow momentum distributions of reaction products in the processes of nuclear break-up and Coulomb dissociation.

A long isotopic chain of carbon nuclei was extensively studied both experimentally and theoretically with the aim to understand the evolution of the nuclear structure as one approaches the drip line. Among other topics, the variation of the nuclear shape with the neutron excess, the development of a halo, and the change of the shell structure are important subjects in the study of the nuclei of carbon isotopes. Recently, an experimental evidence for a prevalent $Z = 6$ magic number in neutron rich carbon isotopes was

*Corresponding author
Email address: Dobrovolsky_AV@pnpi.nrcki.ru (A.V. Dobrovolsky)
[1] Present address: Institute of Modern Physics, Chinese Academy of Sciences, 509 Nanchang Rd., Lanzhou 730000, China
[2] Present address: Department of Physics, Central Michigan University, Mount Plesant, MI 48859, USA
[3] Present address: ISOLDE, CERN, CH-1211 Geneva 23, Switzerland
[4] Present address: Graduate School of Science and Technology, Niigata University, Niigata 950-2102, Japan
[5] Present address: Institut für Kernphysik, Technische Universität Darmstadt, 64289 Darmstadt, Germany

presented [5] based on a systematic study of proton radii, electromagnetic transition rates and atomic masses of light nuclei. Small neutron separation energies are known in ^{15}C, ^{17}C, ^{19}C and ^{22}C [6], so these nuclei are suggested to be candidates to exhibit a neutron halo. Large enhancements in the values of the root-mean-square (rms) nuclear matter radius $R_{\rm m}$ evaluated from the measured interaction cross sections were found for ^{15}C, ^{19}C [7, 8] and ^{22}C [9]. These results also signal the formation of a neutron halo. Narrow fragment momentum distributions of the reaction products in the nuclear break-up of ^{15}C [10–13], ^{19}C [13–15] and ^{22}C [15] support the existence of a halo structure in these nuclei.

The situation concerning a halo formation in ^{17}C is rather contradictory. In several experimental studies a broad momentum distribution observed from the one-neutron nuclear break-up of ^{17}C contradicts a halo existance in this nucleus [10, 11, 13, 14]. This was explained by a d-wave nature of the valence neutron in its ground state. The matter radius derived from the interaction cross section measured at 965 MeV/u did not show a significant enhancement in respect to its neighbours [7]. On the other hand, such an enhancement was predicted in theoretical studies of the properties of the nuclear structure of carbon isotopes [16] within the relativistic Hartree-Fock-Bogolubov theory. The authors of Ref. [16] suggest single-neutron halo structures in both ^{17}C and ^{19}C nuclei. The reaction cross section for scattering of ^{17}C on a ^{12}C target was measured at 79 MeV/u at RIKEN [17]. On the basis of the finite-range Glauber model, the density distribution in ^{17}C was derived using the measured reaction cross section together with the interaction cross section deduced at high energy. From these results a long tail in the neutron density distribution in ^{17}C [17] was suggested. Later, the same experimental data were reanalysed [18] using the well tested modified Glauber model [19]. The results of the analysis [18] showed that ^{17}C is a halo-like nucleus with a big deformation and a tail structure. The deformation may explain the broad momentum distribution of ^{16}C fragments from ^{17}C [18].

The information on the structure of ^{16}C is also contradictory. In an experiment at RIKEN [20], the reaction cross section for scattering of ^{16}C projectiles on a ^{12}C target was measured at an energy of 83 MeV/u. The analysis of the data suggests that ^{16}C has a (core + $2n$) structure and demonstrates the formation of a neutron halo [20]. This would explain an enhancement of the ^{16}C reaction cross section at low energy [20] and an enhancement of the ^{16}C interaction cross section measured at relativistic energy at GSI [7]. The same conclusion about the halo formation in ^{16}C was also drawn in Ref. [21], where a strong prolate deformation of this nucleus was predicted. However, the ^{16}C nucleus has a relatively large neutron separation energy, $S_{2\rm n} = 5.468$ MeV [6], which is not consistent with the existence of a halo in this nucleus. Later, it was found [22] that the momentum distribution of ^{14}C fragments from the ^{16}C break-up is rather broad with a FWHM of 142 ± 14 MeV/c, which also contradicts a halo formation in ^{16}C. Recently new calculations on the structure of the ^{15}C and ^{16}C nuclei [23] lead the author to the conclusion that ^{15}C is a halo nucleus, while ^{16}C has a skin structure.

Probing the nuclear matter distributions in stable nuclei with proton elastic scattering at intermediate energies near 1 GeV is known to be a well established method [3, 24, 25]. In order to study the structure of exotic nuclei, experiments in inverse kinematics were proposed [26] and performed by the PNPI-GSI collaboration at energies of secondary beams around 700 MeV/u at GSI, Darmstadt [27–34]. In these experiments, the hydrogen filled ionization chamber IKAR [27, 28, 35] was used as an active target to measure with high accuracy the absolute differential cross sections for proton elastic small-angle scattering on exotic nuclei. An analysis of the measured cross sections using the Glauber multiple scattering theory makes it possible to study the nuclear matter distributions and to determine the rms of the total matter radii and the radii of the nuclear cores and halos [26, 29]. Previously, the method was applied to study the neutron rich nuclei ^{6}He, ^{8}He, ^{8}Li, ^{9}Li, ^{11}Li, ^{12}Be, ^{14}Be [27–32], and the proton rich nuclei ^{7}Be and ^{8}B [33, 34]. Measurements on the stable nuclei ^{4}He and ^{6}Li, which have equal numbers of protons (Z) and neutrons (N), and for which the difference between the neutron and proton distributions is expected to be small, were used to make a consistency check of the experimental method [29, 31].

In the present experiment, the ^{12,14,15,16,17}C nuclei of the carbon isotopic chain were investigated employing the same method of the proton elastic scattering in inverse kinematics. The aim of the experiment was to obtain the nuclear matter density distributions in the $^{14-17}$C isotopes and to study a possible halo structure in $^{15-17}$C. The ^{14}C nucleus was chosen as a presumable core for the ^{15}C and ^{16}C nuclei. The measurement of the differential cross section for elastic p^{12}C scattering was used as a consistency check of the experimental method, including the data analysis procedure.

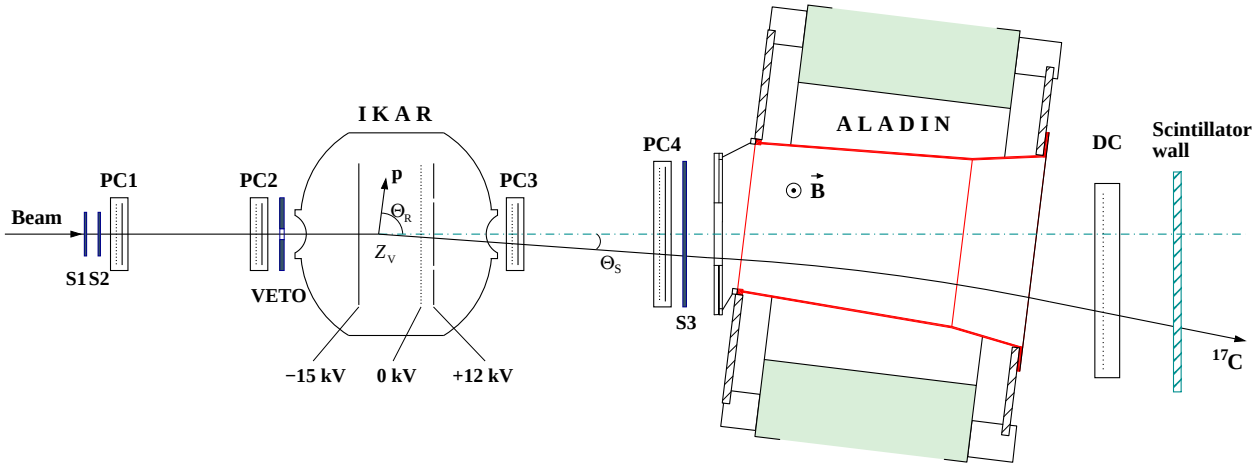

Figure 1: Schematic view of the experimental set-up for small-angle proton elastic scattering in inverse kinematics. The ionization chamber IKAR serves simultaneously as a hydrogen target and a detector for the recoil protons. For the sake of simplicity only one chamber module of six identical ones is shown. In each module the recoil energy T_R, the recoil angle Θ_R and the vertex point Z_V of the interaction are determined. The scattering angle Θ_S of the projectile is determined with four multi-wire proportional chambers PC1–PC4.The scintillator detectors S1–S3 and VETO are used for beam identification and triggering. The scattered projectiles are identified using the ALADIN magnet with the drift chamber (DC) and the scintillator wall, thus separating the break-up reaction products.

2. Experimental set-up and the measurement procedure

The experiment was performed at GSI, Darmstadt. A primary ^{22}Ne beam produced by the UNILAC-SIS accelerator complex was focused on an 8 g/cm^2 Be production target at the entrance of the fragment separator FRS [36]. The carbon isotopes of interest were separated according to their magnetic rigidity and to their nuclear charge by inserting an achromatic (2.7 g/cm^2) aluminium degrader at the dispersive central focal plane of the FRS. The energy of the secondary beam at the centre of the hydrogen target was ∼700 MeV/u with an energy spread of ∼1.3%. The mean energies of the beam particles were determined with an accuracy of about 0.1%. The beam intensity was about 3000 ions/s.

A schematic view of the experimental set-up is shown in Fig. 1. The set-up was the same as in the previous experiment [32]. The main constituent of the set-up was the active target IKAR – an ionization chamber filled with pure hydrogen at a pressure of 10 bar, which served simultaneously as a gas target and a recoil proton detector. IKAR was developed at PNPI [35, 37, 38] and was originally used in experiments on small-angle hadron elastic scattering. The chamber consists of six identical modules. Each module is an axial ionization time-projection chamber, which contains an anode plate (subdivided into a central circular electrode and a concentric ring electrode), a cathode plate, and a grid, all electrodes being arranged perpendicular to the beam direction. At the applied high voltages and for the gas pressure used the electron drift time from the cathode to the grid is 23 μs. The signals from the electrodes provide the energy T_R of the recoil proton (or its energy loss in case it leaves the active volume), the scattering angle Θ_R of the recoil proton, and the coordinate Z_V of the interaction point along the chamber axis in the grid-cathode space [28]. The energy resolution of IKAR was ∼45–55 keV (sigma). The recoil protons were registered in IKAR in coincidence with the scattered projectile particles. The momentum transfer could be determined either from the measured recoil energy T_R or from the value of the scattering angle Θ_S of the projectiles which was measured by a tracking detector system consisting of 2 pairs of two-dimensional multi-wire proportional chambers PC1–PC2 and PC3–PC4, arranged upstream and downstream with respect to IKAR. The corresponding scattering angle Θ_S was obtained using the measured x and y coordinates in the multi-wire proportional chambers. The resolution for the scattering angle was determined by the position resolution of the proportional chambers and the angular spread due to multiple Coulomb scattering of the projectiles. The total angular resolution was estimated to be in the range from $\sigma_\Theta = 0.6$ mrad for the case of

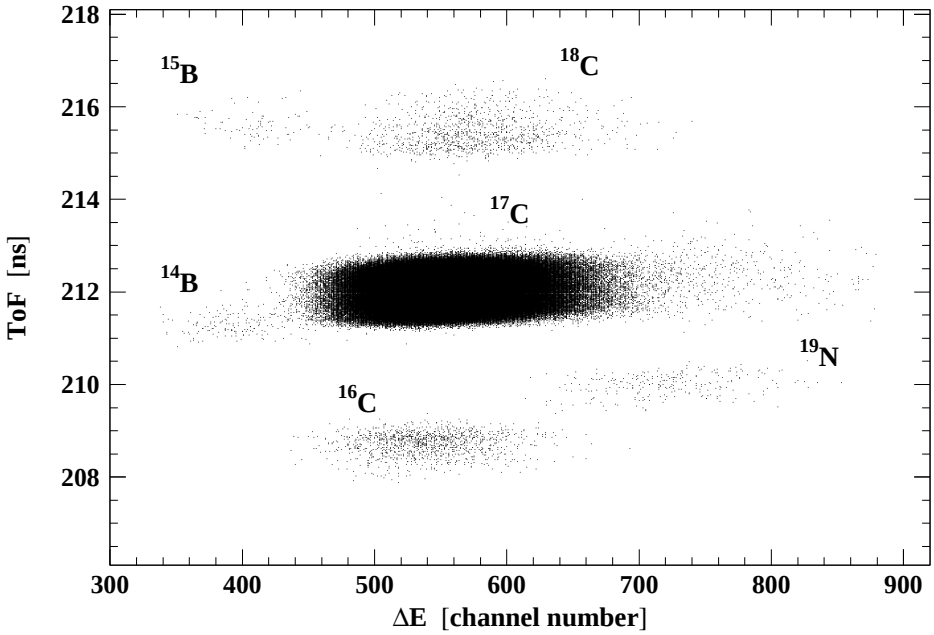

Figure 2: 2-Dimensional plot of the time-of-flight (ToF) and the energy loss (ΔE) in the S3 scintillator for the case of the ^{17}C beam.

^{17}C to $\sigma_\Theta = 0.85$ mrad for ^{12}C, as deduced from calibration measurements with unscattered beam particles.

A set of scintillation counters (S1, S2, S3 and VETO) was used for triggering and identification of the beam particles *via* time-of-flight (ToF) and energy loss (ΔE) measurements. The identification plot for the case of the ^{17}C secondary beam is shown in Fig. 2. The time-of-flight and energy loss of the projectiles in the scintillators allow for unambiguous discrimination of the different isotopes present in the beam. The contamination with other nuclei for each selected carbon isotope was below the 0.1% level.

The ALADIN magnet with a drift chamber and a scintillator wall behind it was utilized to discriminate against break-up reaction channels using magnetic rigidity and energy loss of the reaction products. A detailed description of the experimental set-up and the procedure of the measurement is presented in Refs. [28–34].

The absolute differential cross section $\mathrm{d}\sigma/\mathrm{d}t$ was determined after the event selection using the relation

$$\frac{\mathrm{d}\sigma}{\mathrm{d}t} = \frac{\mathrm{d}N}{\mathrm{d}t B n \Delta L} \, . \tag{1}$$

Here, $\mathrm{d}N$ is the number of elastic proton-nucleus scattering events in the interval $\mathrm{d}t$ of the four-momentum transfer squared, B is the corresponding number of beam particles impinging on the target, n is the density of the hydrogen nuclei known from the measured gas pressure and temperature, and ΔL is the effective target length. The value of t was calculated as $|t| = 2mT_\mathrm{R}$, (where m is the mass of the proton) for the lower momentum transfers, or as $|t| = 4p^2\sin^2(\Theta_\mathrm{S}/2)/(1 + 2E\sin^2(\Theta_\mathrm{S}/2)/m)$ (where p and E denote the projectile initial momentum, and total energy, correspondingly) for the higher momentum transfers [34].

The procedure of the selection of elastic events was the same as in the previous experiments with IKAR [28, 31, 32, 34]. To reject background events, the correlation between the energy E_IKAR deposited in IKAR by the recoil proton and the scattering angle Θ_S of the projectile was used. The measured differential cross sections are to a large extent cross sections for elastic scattering. However, they may contain some admixture of inelastic scattering. Possible contributions of inelastic scattering to the measured cross sections were estimated by calculations.

The calculations of the inelastic cross sections for proton scattering off the carbon isotopes under study were performed using the eikonal model. In particular, the formalism of Ref. [39] was adopted as a starting

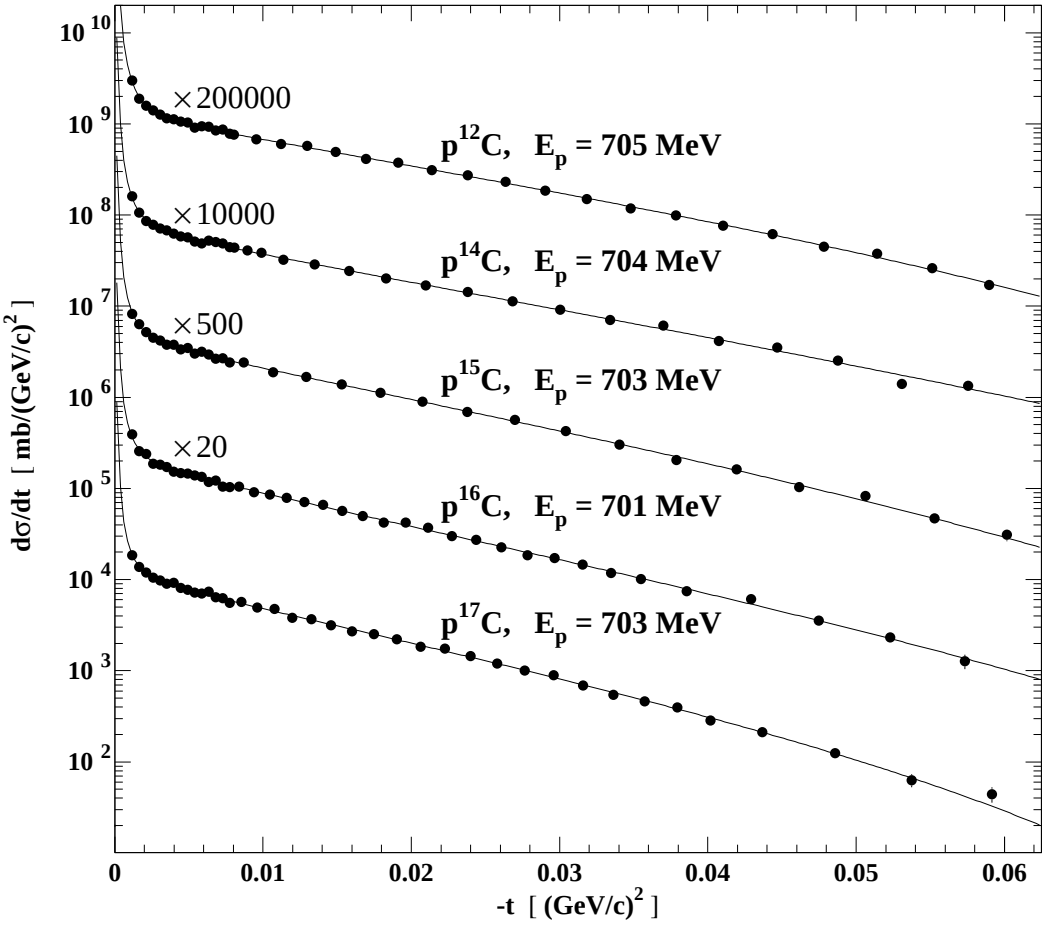

Figure 3: Absolute differential cross sections $\mathrm{d}\sigma/\mathrm{d}t$ for $p^{12,14,15,16,17}$C elastic scattering versus the four-momentum transfer squared $-t$. The indicated energies correspond to the equivalent proton energies for direct kinematics. Solid lines are the results of fits to the experimental cross sections performed within the Glauber theory using the GH parameterization with the fitted parameters.

point, but it was extended in order to distinguish between scattering on protons and neutrons in the nuclei under investigation. Note that for the case of neutron-rich nuclei, such a distinction is obviously necessary. In the calculations, the basic inputs were the nucleon-nucleon (NN) scattering amplitudes and the ground-state (transition) densities for the cases of elastic (inelastic) scattering, respectively. The parameters of the NN amplitudes were taken from Ref. [40]. The ground-state densities were described as Gaussians, while the transition densities were as in the Tassie model [41]. The total differential inelastic cross sections for the different carbon isotopes were calculated by summing up the contributions of all experimentally known states below the particle threshold [42]. The deformation parameters β_{p} and β_{n} used in the calculations were based on the existing experimental information (proton or other scattering data, Coulomb excitation or electromagnetic decay properties). The details of the calculations will be published elsewhere [43].

The calculated inelastic cross sections are significantly smaller than the measured values of $\mathrm{d}\sigma/\mathrm{d}t$ and make a noticeable contribution to $\mathrm{d}\sigma/\mathrm{d}t$ (up to about 10%) only at the highest values of $|t|$ (at $|t| \simeq 0.06$ (GeV/c)^2). The absolute differential cross sections $\mathrm{d}\sigma/\mathrm{d}t$ deduced in the present experiment according to Eq. (1) for proton elastic scattering on the ^{12}C, ^{14}C, ^{15}C, ^{16}C, and ^{17}C nuclei in the momentum-transfer range of $0.002 \leq |t| \leq 0.06$ (GeV/c)^2 after subtraction of the calculated contributions from the inelastic scattering are displayed in Fig. 3 and listed in a tabular form in the Appendix. The indicated energies E_{p} correspond to the equivalent proton energies in direct kinematics. A high detection efficiency for the

beam particles and the elastic-scattering events provide the 2% accuracy of the absolute normalization of the measured cross sections. The uncertainty in the t-scale calibration is estimated to be about 1.5%. Note that the above discussed procedure of subtraction of the estimated contributions of the inelastic scattering had a rather small effect (within the error bars) on the deduced radii.

3. The data analysis and results

The Glauber multiple-scattering theory was applied to establish the nuclear density distributions from the measured cross sections similarly as in Refs. [29–34]. The calculations were performed using the basic Glauber formalism for proton-nucleus elastic scattering and taking experimental data on the elementary proton-proton and proton-neutron scattering amplitudes as input (for details see Ref. [29]). In the analysis of the experimental data, the nuclear many-body density $\rho_{\rm A}$ was taken as a product of the one-body densities, which were parameterized with different functions. The parameters of these densities were found by fitting the calculated cross sections to the experimental data. The fitting procedure is described in detail in Ref. [29].

In order to reduce the model dependence of the obtained results, four parameterizations of phenomenological nuclear density distributions were applied in the present analysis, labeled as SF (Symmetrized Fermi), GH (Gaussian-Halo), GG (Gaussian-Gaussian) and GO (Gaussian-Oscillator). Each of these parameterizations has two free parameters. In the SF parameterization, the free parameters are the so-called "half density radius" R_0 and the diffuseness parameter a. The corresponding rms matter radius $R_{\rm m}$ is connected with the parameters R_0 and a by the relation

$$R_{\rm m} = (3/5)^{1/2}\, R_0\, [1 + (7/3)(\pi a/R_0)^2]^{1/2}. \tag{2}$$

The GH parameterization is determined as a function of the matter radius $R_{\rm m}$ and the halo parameter α, which varies from 0 to 0.4. The case $\alpha = 0$ corresponds to a Gaussian shape, and the one with $\alpha = 0.4$ to a distribution with a pronounced halo component.

While the SF and GH parameterizations do not make any difference between the core and valence neutrons (halo) distributions, the GG and GO parameterizations assume that the nuclei consist of core nucleons and valence nucleons with different spatial distributions. The core distribution is assumed to be a Gaussian one in both the GG and GO parameterizations. The valence nucleon density is described by a Gaussian or a $1p$ shell harmonic oscillator-type distribution within the GG or GO parameterizations, respectively. The free parameters in the GG and GO parameterizations are the rms radii $R_{\rm c}$ and $R_{\rm v}$ ($R_{\rm h}$) of the core and valence ("halo") nucleon distributions. The matter radius $R_{\rm m}$ is connected with $R_{\rm c}$ and $R_{\rm v}$ by the following relation:

$$R_{\rm m} = [(A_{\rm c}R_{\rm c}^2 + A_{\rm v}R_{\rm v}^2)/A]^{1/2}, \tag{3}$$

where A is the nuclear mass number, $A_{\rm c}$ is the number of nucleons in the core, and $A_{\rm v}$ is the number of valence nucleons. The explicit expressions for the SF, GH, GG and GO parameterizations are given in Ref. [29].

The results of the fits to the measured experimental cross sections with the phenomenological density distributions SF, GH, GG and GO for the carbon isotopes under investigation are presented in Table 1. For each density parameterization, the deduced rms nuclear matter radius $R_{\rm m}$, the χ^2 value of the fitting procedure, the values of the fit parameters, and the normalization coefficient $A_{\rm n}$ with which the calculated cross section ${\rm d}\sigma/{\rm d}t$ was multiplied to obtain the same absolute normalization as the experimental one are presented. Note that the errors in Table 1 are statistical only.

The solid lines in Fig. 3 represent the results for the cross sections ${\rm d}\sigma/{\rm d}t$ calculated using the GH parameterization with the fitted parameters. At $|t| < 0.005$ $({\rm GeV}/c)^2$, a steep rise of the cross section with decreasing $|t|$ is caused by Coulomb scattering. It is seen that the fits describe the experimental cross sections fairly well with the reduced χ^2 values close to 1.0. The calculations of the cross sections with the nuclear matter density parameterizations SF, GG, and GO with the fitted parameters give practically the same results.

Table 1: Parameters obtained by fitting the calculated proton elastic scattering cross sections for the carbon isotopes under investigation to the measured cross sections for the parameterizations SF, GH, GG and GO of the nuclear matter density distributions. The presented parameters refer to point-nucleon density distributions. $A_{\rm n}$ denotes the normalization factor of the calculated cross section, $N_{\rm df}$ is the number of degrees of freedom. $A_{\rm n}$, $\chi^2/N_{\rm df}$ and α are dimensionless, all other fit parameters are given in fm. The radii $R_{\rm c}$ and $R_{\rm v}$ are in the c.m. system of the nucleus. All errors given are statistical only.

Nucleus	Parameterization	$\chi^2/N_{\rm df}$	Fit parameters			$R_{\rm m}$, fm
			$A_{\rm n}$	Density parameters		
^{12}C	SF	30.0/33	1.03(1)	$R_0 = 1.98(13)$	a = 0.48(3)	2.35(2)
	GH	30.2/33	1.03(1)	$R_{\rm m} = 2.33(1)$	$\alpha = 0.00(2)$	2.33(1)
^{14}C	SF	31.1/31	1.01(1)	$R_0 = 0.87(32)$	a = 0.63(3)	2.43(2)
	GH	31.4/31	1.01(1)	$R_{\rm m} = 2.41(2)$	$\alpha = 0.11(2)$	2.41(2)
^{15}C	SF	32.6/29	1.03(1)	$R_0 = 1.56(16)$	a = 0.62(2)	2.59(2)
	GH	32.6/29	1.03(1)	$R_{\rm m} = 2.57(2)$	$\alpha = 0.06(2)$	2.57(2)
	GG	34.4/29	1.02(1)	$R_{\rm c} = 2.43(1)$	$R_{\rm v} = 4.45(43)$	2.61(5)
	GO	33.6/29	1.02(1)	$R_{\rm c} = 2.40(1)$	$R_{\rm v} = 4.49(33)$	2.60(4)
^{16}C	SF	33.5/37	1.04(1)	$R_0 = 1.31(25)$	a = 0.67(3)	2.70(3)
	GH	36.3/37	1.04(1)	$R_{\rm m} = 2.68(3)$	$\alpha = 0.09(2)$	2.68(3)
	GG	35.3/37	1.04(1)	$R_{\rm c} = 2.43(2)$	$R_{\rm v} = 4.36(29)$	2.75(6)
	GO	35.0/37	1.04(1)	$R_{\rm c} = 2.38(2)$	$R_{\rm v} = 4.35(22)$	2.71(4)
^{17}C	SF	35.0/37	1.01(1)	$R_0 = 1.97(13)$	a = 0.60(2)	2.69(2)
	GH	34.7/37	1.02(1)	$R_{\rm m} = 2.67(2)$	$\alpha = 0.03(2)$	2.67(2)
	GG	35.5/37	1.02(1)	$R_{\rm c} = 2.58(2)$	$R_{\rm v} = 3.86(54)$	2.68(3)
	GO	35.3/37	1.02(1)	$R_{\rm c} = 2.56(2)$	$R_{\rm v} = 4.06(40)$	2.67(3)

For the description of the cross sections in the case of the ^{12}C and ^{14}C nuclei, only the SF and GH density parameterizations were used. The weighted mean values of $R_{\rm m}$ averaged over the results obtained with these density parameterizations are:

$$R_{\rm m} = (2.34 \pm 0.05)\ \text{fm} \qquad \text{for } ^{12}\text{C},$$
$$R_{\rm m} = (2.42 \pm 0.05)\ \text{fm} \qquad \text{for } ^{14}\text{C}.$$

The errors indicated here and below for the deduced values of the radii include statistical and systematic uncertainties. The systematic errors appear due to uncertainties in the absolute normalization of the experimental cross sections, errors introduced to the analysis from uncertainties in the parameters of the free *pp* and *pn* scattering amplitudes, and corrections for the inelastic scattering contributions, uncertainties due to different model density parameterizations used, and the error in the t-scale. For details see [29].

In the analysis it was assumed that the nuclei ^{15}C and ^{17}C consist of the ^{14}C, and ^{16}C cores, respectively, and a loosely bound valence neutron. For these nuclei good descriptions of the cross sections have been achieved with all the density parameterizations used. The corresponding values of the rms matter radii $R_{\rm m}$ deduced with all four parameterizations for ^{15}C and ^{17}C are close to each other within rather small errors. The values of $R_{\rm m}$ averaged over the results obtained with all the density parameterizations are:

$$R_{\rm m} = (2.59 \pm 0.05)\ \text{fm} \qquad \text{for } ^{15}\text{C},$$
$$R_{\rm m} = (2.68 \pm 0.05)\ \text{fm} \qquad \text{for } ^{17}\text{C}.$$

The mean value for the core radius of ^{15}C deduced with the GG and GO parameterizations is $R_{\rm c} = 2.41(5)$ fm. Combining the obtained values of $R_{\rm m}$ and $R_{\rm c}$, and employing relation (3) between the rms radii $R_{\rm m}$, $R_{\rm c}$, and $R_{\rm v}$, one derives for the radius of the valence neutron distribution in ^{15}C a value of $R_{\rm v} = 4.36(38)$

fm. The mean values of the core radius and the radius of the valence neutron distribution deduced in the present analysis for ^{17}C are $R_c = 2.57(5)$ fm and $R_v = 4.05(47)$ fm.

In the analysis of the data for the ^{16}C nucleus with the density parameterization within the GG and GO models a structure of a ^{14}C core plus two valence neutrons was assumed. For this isotope all density parameterizations also fit the experimental data well. The weighted mean rms matter radius of ^{16}C, deduced from the GH, SF, GG, and GO parameterizations is

$$R_m = (2.70 \pm 0.06) \text{ fm}.$$

For the core radius and the radius of the valence neutrons distribution, the following mean values were determined: $R_c = 2.41(5)$ fm and $R_v = 4.20(26)$ fm.

The deduced nuclear matter density distributions obtained using different parameterizations of the nuclear matter distributions are plotted in Fig. 4. The shaded areas represent the envelopes of the density variation within the model parameterizations applied, superimposed by the statistical errors. Figure 4 also shows the obtained core matter distributions. All density distributions refer to point-nucleon distributions.

Using the matter radii R_m deduced in the present work and the radii R_p of proton distributions obtained in Refs. [44] and [8], the radii R_n of neutron distributions and thicknesses of the neutron skins $\delta_{np} = R_n - R_p$ for the nuclei of the studied carbon isotopes were determined (see Table 2) with the help of expression (4):

$$R_n = [(AR_m^2 - ZR_p^2)/N]^{1/2}. \quad (4)$$

4. Discussion

Recently, the charge-changing cross sections for the $^{12-19}$C nuclei were measured at GSI at 900 MeV/u with a carbon target by Kanungo *et al.* [8]. Using a finite-range Glauber model, the authors derived radii R_p of the proton density distributions for the studied carbon isotopes. With these values of R_p fixed, they performed a new analysis of the interaction cross sections from Ref. [7] to obtain more accurate values of the matter radii R_m. The authors also performed coupled-cluster computations using chiral nucleon-nucleon and three-nucleon interactions which satisfactorily describe the experimental data on proton and matter radii.

Our results on R_m for the carbon isotopes are compared with the results of Ref. [8] in Table 2 and in Fig. 5. Two sets of theoretical predictions for the matter radii of the carbon isotopes [45, 46] are also shown in Fig. 5. The present results of R_m turn out to be within the experimental errors in agreement with the results of Ref. [8].

The method applied in the given work to study the nuclear matter density distributions was previously tested with the data on proton scattering from stable nuclei ^{4}He [29] and ^{6}Li [31]. The differential cross section for p^{12}C elastic scattering measured in this work was also used to check the method. The ^{12}C matter radius $R_m = 2.34(5)$ fm derived in the present work is in agreement with the value of $R_m = 2.35(2)$ fm of Ref. [8]. Note that the rms charge radius of ^{12}C is known with a high precision [44] from e^- scattering and

Table 2: Comparison of the present results on the rms radii of the nuclear matter with the values derived from the Glauber analysis of interaction cross sections [8]. In addition data on the radius of the proton distribution R_p (from refs. [8] and [44]) and on the deduced radii of the neutron distribution R_n and of the thickness of the neutron skin δ_{np} are presented.

Isotope	R_m, fm	R_m, fm	R_p, fm		R_n, fm	δ_{np}, fm
	This work	Ref. [8]	Ref. [44]	Ref. [8]	This work	This work
^{12}C	2.34 (5)	2.35 (2)	2.34 (1)		2.34 (10)	0.00 (10)
^{14}C	2.42 (5)	2.33 (7)	2.38 (2)		2.45 (9)	0.07 (9)
^{15}C	2.59 (5)	2.54 (4)		2.37 (3)	2.73 (8)	0.36 (9)
^{16}C	2.70 (6)	2.74 (3)		2.40 (4)	2.86 (9)	0.46 (10)
^{17}C	2.68 (5)	2.76 (3)		2.42 (4)	2.81 (8)	0.39 (9)

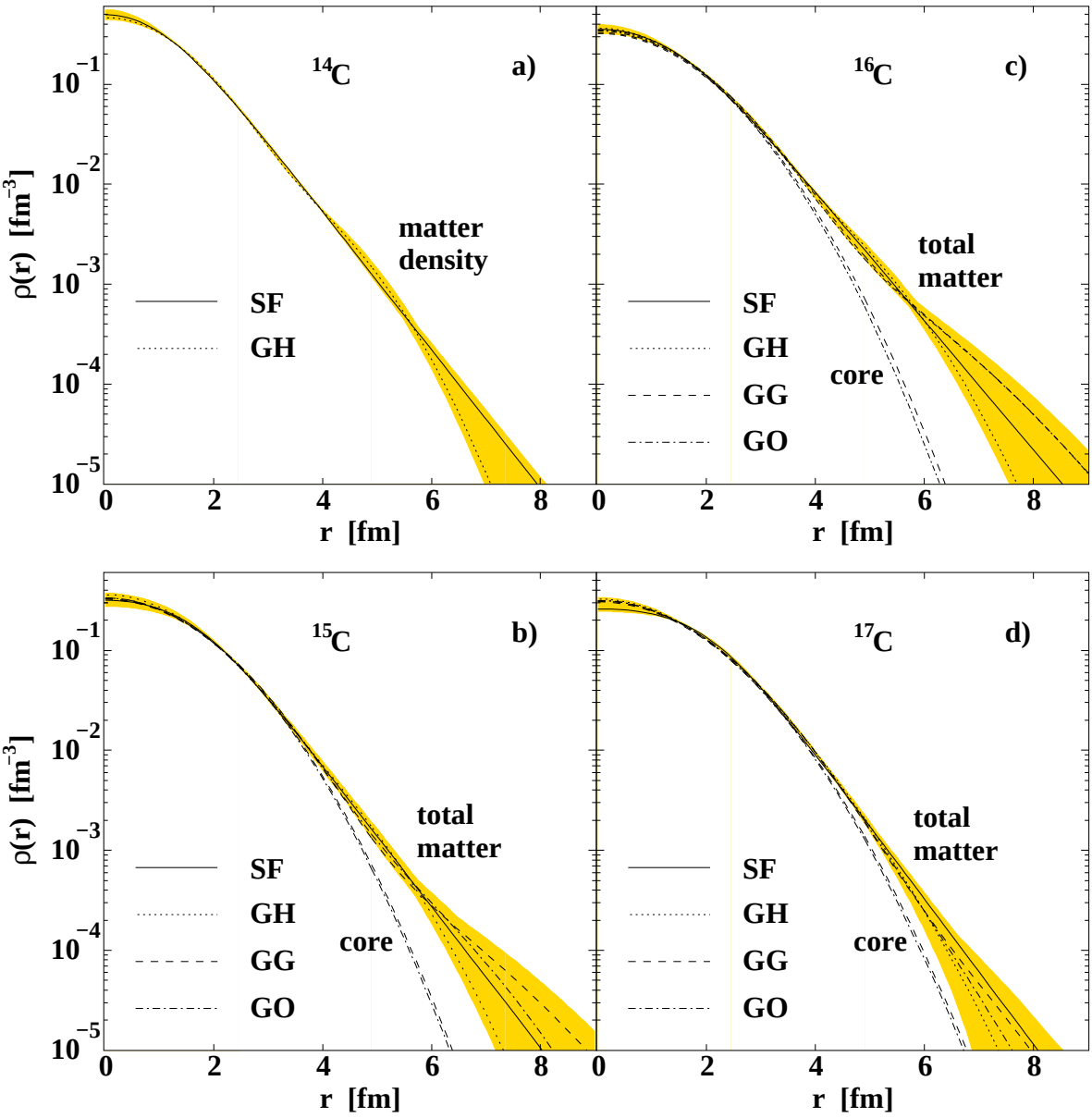

Figure 4: Total and core matter distributions $\rho(r)$ of the nuclear density in ^{14}C (a), ^{15}C (b), ^{16}C (c) and ^{17}C (d) deduced by using different model parameterizations in the analysis. The shaded areas represent the envelopes of the density variation within the model parameterizations applied, superimposed by the statistical errors. All density distributions are normalized to the number of nucleons.

muonic x-ray measurements: $R_{\rm ch} = 2.470(2)$ fm. Taking into account the finite size effect of the nucleon (see, *e.g.*, Ref. [3]) and the value of the proton charge radius $r_{\rm p} = 0.8414(19)$ fm [47], the rms radius $R_{\rm p}$ of the proton distribution in ^{12}C is obtained to be $R_{\rm p} = 2.34(1)$ fm. The number of neutrons in ^{12}C is equal to that of protons, therefore the matter and proton distributions (normalized to one nucleon) are expected to be rather similar. Indeed, the $R_{\rm m}$ value deduced in the present work has occurred to be equal to the value of $R_{\rm p}$ extracted from the experimental data on the charge radius of ^{12}C. This result on p^{12}C scattering demonstrates a consistency check of the present experimental method, including the procedure of the data analysis.

The ^{14}C nucleus is of interest as the presumable core in ^{15}C and ^{16}C [5]. This nucleus is supposed to have a spherical shape due to the neutron closed shell effect [48–50]. The present value of $R_{\rm m} = 2.42(5)$ fm is in agreement within errors with the result $R_{\rm m} = 2.33(7)$ fm of Ref. [8]. The charge radius $R_{\rm ch} = 2.503(9)$ fm [44] of ^{14}C may be used to find the corresponding radius of the proton distribution $R_{\rm p} = 2.38(2)$ fm. By combining the matter radius $R_{\rm m}$, deduced in the present work for ^{14}C with the value of $R_{\rm p}$, and using expression (4), the rms radius of the neutron distribution $R_{\rm n}$ in ^{14}C has been determined to be $R_{\rm n} = (2.45 \pm 0.09)$ fm. Thus, within the error bars, the ^{14}C nucleus has the same radius of the neutron distribution $R_{\rm n}$ as that of the proton distribution $R_{\rm p}$.

The structure of the odd isotope ^{15}C has been considered in a (^{14}C-core + n) model. This nucleus has a small neutron separation energy $S_{\rm n} = 1.218$ MeV, so it is suggested to be a candidate for a halo nucleus. A special feature of the present method is that it makes possible to determine the sizes of the nuclear core and of the halo. The ratio of the determined valence nucleon to the core nucleon radius, $\kappa = R_{\rm v}/R_{\rm c}$, may be used as a gauge for the halo existence [51]. Theory predicts typically values of $\kappa \leq 1.25$ for light nuclei near the valley of beta stability, while for a halo structure this value can be $\kappa \approx 2$, or even larger [2]. In the present analysis, a value of $\kappa = 1.81$ for ^{15}C is obtained, which confirms the suggestion [3] that this nucleus demonstrates a "moderate halo formation".

Due to the low binding energy of the halo neutron in ^{15}C, it is natural to expect that the internal core size $R_{\rm c}^*$ (size of the core in its own c.m. system) is close to that of the free ^{14}C nucleus. The motion of the c.m. of the core around the c.m. of the whole nucleus slightly increases the effective core size $R_{\rm c}$ [29]. Following Tanihata *et al.* [3], the internal core size $R_{\rm c}^*$ in the (core + n) model turns out to be

$$R_{\rm c}^* = (R_{\rm c}^2 - \rho_{\rm c}^2)^{1/2}, \tag{5}$$

where $\rho_{\rm c}$ is the rms distance between the c.m. of the core and the c.m. of the whole nucleus:

$$\rho_{\rm c} = R_{\rm v}/(A-1). \tag{6}$$

In the present analysis we obtain $\rho_{\rm c} = 0.31(2)$ fm and $R_{\rm c}^* = 2.39(5)$ fm for ^{15}C. The latter value agrees with $R_{\rm m} = 2.42(5)$ fm for ^{14}C. Taking for ^{15}C the proton radius $R_{\rm p} = (2.37 \pm 0.03)$ fm [8], and using Eq. (4), the rms neutron radius for ^{15}C is determined to be $R_{\rm n} = (2.73 \pm 0.08)$ fm, and for the thickness of the neutron skin we deduce the value of $\delta_{\rm np} = (0.36 \pm 0.09)$ fm (see Table 2).

There are several theoretical considerations of the structure of ^{16}C, which is treated as a (^{14}C-core $+n+n$) three-body system [45, 46]. The experimental value of $R_{\rm m} = 2.70(6)$ fm, deduced in the present work for ^{16}C, is in good agreement with existing experimental data as well as with theoretical results (Fig. 5 and Table 2). According to the present analysis, the ratio of the valence nucleon radius $R_{\rm v}$ to the core radius $R_{\rm c}$ turns out to be equal in this nucleus to $\kappa = 1.74$, which is smaller than the κ values of the $2n$ halo nuclei ^{11}Li ($\kappa = 2.71$ [31]) and ^{14}Be ($\kappa = 1.91$ [32]) determined earlier with the same method. This observation suggests that the spatial distribution of two valence neutrons in ^{16}C should be considered rather as a skin, than as a halo. Using the matter radius of the present work $R_{\rm m} = (2.70 \pm 0.06)$ fm and the radius of the proton distribution $R_{\rm p} = (2.40 \pm 0.04)$ fm [8], we obtain for the radius of the neutron distribution $R_{\rm n} = (2.86 \pm 0.09)$ fm, and for the thickness of the neutron skin, the value $\delta_{\rm np} = (0.46 \pm 0.10)$ fm has been deduced (see Table 2). This result is an indication of a noticeable neutron skin in ^{16}C.

We have considered the spatial structure of the ^{17}C nucleus in a (^{16}C-core + n) model. The neutron separation energy $S_{\rm n}$ for ^{17}C is small: $S_{\rm n} = 0.728$ MeV. Therefore, one could expect ^{17}C to be a halo nucleus. However, the ratio of the valence nucleon radius to the core radius, determined in the present work for ^{17}C,

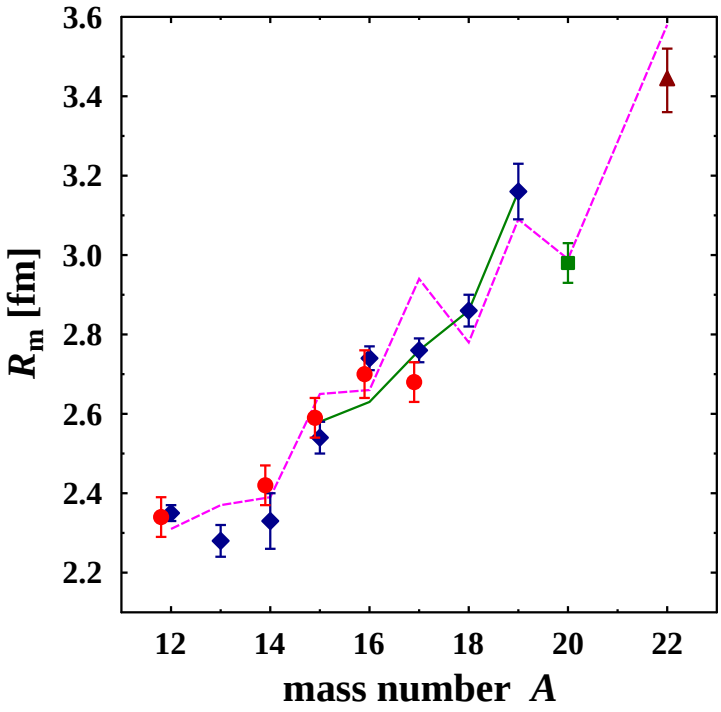

Figure 5: Nuclear matter radii of carbon isotopes. Experimental data are: this work (circles), the results of [8] (diamonds), the result of [4] (square), and the result of [9] (triangle). Theoretical predictions are taken from [45] (solid line) and [46] (dashed line).

occurs to be relatively small, $\kappa = 1.58$, which does not support the picture that ^{17}C is a halo nucleus. With the determined value of $R_{\rm v}$ and Eqs. (5) and (6) in the case of ^{17}C we obtain $\rho_{\rm c} = 0.25$ fm and $R^*_{\rm c} = 2.56(5)$ fm. This value of $R^*_{\rm c}$ is smaller than $R_{\rm m} = 2.70(6)$ fm for a free ^{16}C nucleus. This result demonstrates a noticeable contraction of the ^{16}C cluster inside ^{17}C. Obviously, ^{17}C is a more dense nucleus than ^{16}C. It was already supposed in Ref. [3] that the configuration of the nucleus ^{17}C is more complicated than that in the (core + n) model.

5. Summary

The proton-nucleus elastic scattering at intermediate energies is an efficient method for the investigation of nuclear matter density distributions. In the present work, we have applied this method in inverse kinematics for the investigation of the nuclear radial structure of carbon isotopes. The absolute differential cross sections dσ/dt were measured as a function of the four-momentum transfer squared $-t$ in the range $0.001 \leq |t| \leq 0.06$ (GeV/c)^2 for proton elastic scattering on the ^{12,14,15,16,17}C nuclei. The cross sections were determined using secondary beams from the GSI fragment separator FRS at an energy of ~700 MeV/u. The hydrogen-filled ionization chamber IKAR served simultaneously as a hydrogen target and a recoil-proton detector. The scattered projectiles were registered with a system of multi-wire proportional chambers, scintillation detectors, and a magnetic analysis. The nuclear matter radii and the radial nuclear matter distributions were determined from the measured cross sections dσ/dt with the aid of the Glauber multiple-scattering theory. In the analysis, four phenomenological parameterizations of the nuclear density

distributions (SF, GH, GG, and GO) were used, each of these parameterizations having two free parameters. Our results on the matter radii $R_{\rm m}$ for the studied carbon isotopes are in agreement within the experimental errors with those of Ref. [8] evaluated from the measured interaction and charge-changing cross sections. The density distribution parameters ($R_{\rm m}$, $R_{\rm p}$) for ^{12}C are well established values from measurements of the interaction cross sections and the charge radii. Therefore, the results on p^{12}C scattering were used as a consistency check of the present experimental method, including the procedure of the data analysis.

The measured cross sections are described fairly well within the (core + n) model for ^{15}C and ^{17}C, and the (core + $2n$) model for ^{16}C. It was shown that the size of the ^{14}C-core in the ^{15}C and ^{16}C nuclei is close to that of a free ^{14}C nucleus.

A quantitative description of the halo structure for ^{15,16,17}C was performed in the analysis of the nuclear matter distributions in these nuclei. The ratio of the valence nucleon to the core nucleon radius $\kappa = R_{\rm v}/R_{\rm c}$ was used as a gauge for the halo existence, where a value of $\kappa \gtrsim 2$ is expected for a halo nucleus.

The present analysis describes ^{15}C as a halo nucleus with $\kappa = 1.82$, while ^{16}C ($\kappa = 1.74$) and ^{17}C ($\kappa = 1.58$) are considered as nuclei with a noticeable neutron skin. This conclusion is in agreement with the investigation of fragmentation reactions using radioactive carbon beams. Note that a narrow fragment momentum distribution as a signature of an extended valence nucleon density distribution in a halo nucleus was observed in the considered here carbon isotopes only for ^{15}C [10–13], whereas broad fragment momentum distributions for ^{16}C [22] and ^{17}C [10, 11, 13, 14] imply no halo formation in these nuclei.

Besides the determination of the nucleon density distributions and their parameters, the precise data obtained for the differential proton elastic-scattering cross sections allow a sensitive test of theoretical predictions on the structure of the neutron-rich carbon nuclei. For this purpose, the nuclear density distributions obtained from various theoretical approaches may be used as an input to the Glauber multiple-scattering theory. Then the calculated elastic-scattering cross sections should be compared to the experimental data as it was done in Refs. [29–31].

Acknowledgements

The authors are grateful to A. Bleile, G. Ickert, A. Brünle, K.-H. Behr and W. Niebur for their technical assistance in the preparation of the experimental set-up. The visiting group from PNPI thanks the GSI authorities for the hospitality.

References

[1] I. Tanihata, Neutron halo nuclei, J. Phys. G 22 (1996) 157.
[2] B. Jonson, Light dripline nuclei, Phys. Rep. 389 (2004) 1.
[3] I. Tanihata, H. Savajols, R. Kanungo, Recent experimental progress in nuclear halo structure studies, Prog. Part. Nucl. Phys. 68 (2013) 215.
[4] A. Ozawa, T. Suzuki, I. Tanihata, Nuclear size and related topics, Nuclear Physics A 693 (2001) 32.
[5] D. Tran, H. Ong, G. Hagen, T. Morris, N. Aoi, T. Suzuki, Y. Kanada-Enyo, L. Geng, S. Terashima, I. Tanihata, T. Nguyen, Y. Ayyad, P. Chan, M. Fukuda, H. Geissel, M. Harakeh, T. Hashimoto, T. Hoang, E. Ideguchi, A. Inoue, G. Jansen, R. Kanungo, T. Kawabata, L. Khiem, W. Lin, K. Matsuta, M. Mihara, S. Momota, D. Nagae, N. Nguyen, D. Nishimura, T. Otsuka, A. Ozawa, P. Ren, H. Sakaguchi, C. Scheidenberger, J. Tanaka, M. Takechi, R. Wada, T. Yamamoto, Evidence for prevalent Z = 6 magic number in neutron-rich carbon isotopes, Nature Communications 9 (2018) 1594.
[6] M. Wang, G. Audi, A. Wapstra, F. Kondev, M. MacCormick, X. Xu, B. Pfeiffer, The Ame2012 atomic mass evaluation, Chin. Phys. C 36 (2012) 1603.
[7] A. Ozawa, O. Bochkarev, L. Chulkov, D. Cortina, H. Geissel, M. Hellström, M. Ivanov, R. Janik, K. Kimura, T. Kobayashi, A. Korsheninnikov, G. Münzenberg, F. Nickel, Y. Ogawa, A. Ogloblin, M. Pfützner, V. Pribora, H. Simon, B. Sitár, P. Strmen, K. Sümmerer, T. Suzuki, I. Tanihata, M. Winkler, K. Yoshida, Measurements of interaction cross sections for light neutron-rich nuclei at relativistic energies and determination of effective matter radii, Nuclear Physics A 691 (2001) 599.
[8] R. Kanungo, W. Horiuchi, G. Hagen, G. R. Jansen, P. Navratil, F. Ameil, J. Atkinson, Y. Ayyad, D. Cortina-Gil, I. Dillmann, A. Estradé, A. Evdokimov, F. Farinon, H. Geissel, G. Guastalla, R. Janik, M. Kimura, R. Knöbel, J. Kurcewicz, Y. A. Litvinov, M. Marta, M. Mostazo, I. Mukha, C. Nociforo, H. J. Ong, S. Pietri, A. Prochazka, C. Scheidenberger, B. Sitar, P. Strmen, Y. Suzuki, M. Takechi, J. Tanaka, I. Tanihata, S. Terashima, J. Vargas, H. Weick, J. S. Winfield, Proton Distribution Radii of $^{12-19}$C Illuminate Features of Neutron Halos, Phys. Rev. Lett. 117 (2016) 102501.

[9] Y. Togano, T. Nakamura, Y. Kondo, J. Tostevin, A. Saito, J. Gibelin, N. Orr, N. Achouri, T. Aumann, H. Baba, F. Delaunay, P. Doornenbal, N. Fukuda, J. Hwang, N. Inabe, T. Isobe, D. Kameda, D. Kanno, S. Kim, N. Kobayashi, T. Kobayashi, T. Kubo, S. Leblond, J. Lee, F. Marqus, R. Minakata, T. Motobayashi, D. Murai, T. Murakami, K. Muto, T. Nakashima, N. Nakatsuka, A. Navin, S. Nishi, S. Ogoshi, H. Otsu, H. Sato, Y. Satou, Y. Shimizu, H. Suzuki, K. Takahashi, H. Takeda, S. Takeuchi, R. Tanaka, A. Tuff, M. Vandebrouck, K. Yoneda, Interaction cross section study of the two-neutron halo nucleus ^{22}C, Physics Letters B 761 (2016) 412.

[10] D. Bazin, W. Benenson, B. Brown, J. Brown, B. Davids, M. Fauerbach, P. Hansen, P. Mantica, D. Morrissey, C. Powell, B. Sherrill, M. Steiner, Probing the halo structure of ^{19,17,15}C and ^{14}B, Phys. Rev. C 57 (1998) 2156.

[11] E. Sauvan, F. Carstoiu, N. Orr, J. Winfield, M. Freer, J. Angélique, W. Catford, N. Clarke, N. Curtis, S. Grévy, C. Le Brun, M. Lewitowicz, E. Liégard, F. Marqués, M. Mac Cormick, P. Roussel-Chomaz, M.-G. Saint Laurent, M. Shawcross, One-neutron removal reactions on light neutron-rich nuclei, Phys. Rev. C 69 (2004) 044603.

[12] D. Fang, T. Yamaguchi, T. Zheng, A. Ozawa, M. Chiba, R. Kanungo, T. Kato, K. Morimoto, T. Ohnishi, T. Suda, Y. Yamaguchi, A. Yoshida, K. Yoshida, I. Tanihata, One-neutron halo structure in ^{15}C, Phys. Rev. C 69 (2004) 034613.

[13] C. Rodríguez-Tajes, H. Álvarez-Pol, T. Aumann, E. Benjamim, J. Benlliure, M. J. G. Borge, M. Caamaño, E. Casarejos, A. Chatillon, D. Cortina-Gil, K. Eppinger, T. Faestermann, M. Gascón, H. Geissel, R. Gernhäuser, B. Jonson, R. Kanungo, R. Krücken, T. Kurtukian, K. Larsson, P. Maierbeck, T. Nilsson, C. Nociforo, C. Pascual-Izarra, A. Perea, D. Pérez-Loureiro, A. Prochazka, S. Schwertel, H. Simon, K. Sümmerer, O. Tengblad, H. Weick, M. Winkler, M. Zhukov, One-neutron knockout from light neutron-rich nuclei at relativistic energies, Phys. Rev. C 82 (2010) 024305.

[14] T. Baumann, M. Borge, H. Geissel, H. Lenske, K. Markenroth, W. Schwab, M. Smedberg, T. Aumann, L. Axelsson, U. Bergmann, D. Cortina-Gil, L. Fraile, M. Hellström, M. Ivanov, N. Iwasa, R. Janik, B. Jonson, G. Münzenberg, F. Nickel, T. Nilsson, A. Ozawa, A. Richter, K. Riisager, C. Scheidenberger, G. Schrieder, H. Simon, B. Sitar, P. Strmen, K. Sümmerer, T. Suzuki, M. Winkler, H. Wollnik, M. Zhukov, Longitudinal momentum distributions of ^{16,18}C fragments after one-neutron removal from ^{17,19}C, Physics Letters B 439 (1998) 256.

[15] N. Kobayashi, T. Nakamura, J. A. Tostevin, Y. Kondo, N. Aoi, H. Baba, S. Deguchi, J. Gibelin, M. Ishihara, Y. Kawada, T. Kubo, T. Motobayashi, T. Ohnishi, N. A. Orr, H. Otsu, H. Sakurai, Y. Satou, E. C. Simpson, T. Sumikama, H. Takeda, M. Takechi, S. Takeuchi, K. N. Tanaka, N. Tanaka, Y. Togano, K. Yoneda, One- and two-neutron removal reactions from the most neutron-rich carbon isotopes, Phys. Rev. C 86 (2012) 054604.

[16] X. L. Lu, B. Y. Sun, W. H. Long, Description of carbon isotopes within relativistic Hartree-Fock-Bogoliubov theory, Phys. Rev. C 87 (2013) 034311.

[17] C. Wu, Y. Yamaguchi, A. Ozawa, R. Kanungo, I. Tanihata, T. Suzuki, D. Fang, T. Suda, T. Ohnishi, M. Fukuda, N. Iwasa, T. Ohtsubo, T. Izumikawa, R. Koyama, W. Shinozaki, M. Takahashi, Study of the density distribution of ^{17}C from reaction cross section measurement, Nuclear Physics A 739 (2004) 3.

[18] G.-W. Fan, X.-L. Cai, T.-F. Han, X.-C. Li, Z.-Z. Ren, W. Xu, M. Fukuda, Big deformation in ^{17}C, Chinese Physics C 38 (2014) 014101.

[19] M. Takechi, M. Fukuda, M. Mihara, K. Tanaka, T. Chinda, T. Matsumasa, M. Nishimoto, R. Matsumiya, Y. Nakashima, H. Matsubara, K. Matsuta, T. Minamisono, T. Ohtsubo, T. Izumikawa, S. Momota, T. Suzuki, T. Yamaguchi, R. Koyama, W. Shinozaki, M. Takahashi, A. Takizawa, T. Matsuyama, S. Nakajima, K. Kobayashi, M. Hosoi, T. Suda, M. Sasaki, S. Sato, M. Kanazawa, A. Kitagawa, Reaction cross sections at intermediate energies and Fermi-motion effect, Phys. Rev. C 79 (2009) 061601.

[20] T. Zheng, T. Yamaguchi, A. Ozawa, M. Chiba, R. Kanungo, T. Kato, K. Katori, K. Morimoto, T. Ohnishi, T. Suda, I. Tanihata, Y. Yamaguchi, A. Yoshida, K. Yoshida, H. Toki, N. Nakajima, Study of halo structure of ^{16}C from reaction cross section measurement, Nuclear Physics A 709 (2002) 103.

[21] M. Rashdan, Deformation, orientation, and medium effects in ^{16,19}C + C reactions, Phys. Rev. C 86 (2012) 044610.

[22] T. Yamaguchi, T. Zheng, A. Ozawa, M. Chiba, R. Kanungo, T. Kato, K. Morimoto, T. Ohnishi, T. Suda, Y. Yamaguchi, A. Yoshida, K. Yoshida, I. Tanihata, Momentum distributions of ^{14}C and ^{15}C fragments from ^{16}C breakup, Nuclear Physics A 724 (2003) 3.

[23] M. Rashdan, Analysis of the reaction cross sections of ^{15,16}C + ^{12}C and ^{15,16}C + ^{27}Al at intermediate energies using microscopic optical potential and Glauber model, Eur. Phys. J. A 56 (2020) 130.

[24] G. Alkhazov, S. Belostotsky, A. Vorobyov, Scattering of 1 GeV protons on nuclei, Physics Reports 42 (1978) 89.

[25] H. Sakaguchi, J. Zenihiro, Proton elastic scattering from stable and unstable nuclei Extraction of nuclear densities, Progress in Particle and Nuclear Physics 97 (2017) 1.

[26] G. Alkhazov, A. Lobodenko, Possibility of determining the radius of the neutron halo in light exotic nuclei, JETP Lett. 55 (1992) 379.

[27] G. Alkhazov, M. Andronenko, A. Dobrovolsky, P. Egelhof, G. Gavrilov, H. Geissel, H. Irnich, A. Khanzadeev, G. Korolev, A. Lobodenko, G. Münzenberg, M. Mutterer, S. Neumaier, F. Nickel, W. Schwab, D. Seliverstov, T. Suzuki, J. Theobald, N. Timofeev, A. Vorobyov, V. Yatsoura, Nuclear Matter Distributions in ^{6}He and ^{8}He from Small Angle p-He Scattering in Inverse Kinematics at Intermediate Energy, Phys. Rev. Lett. 78 (1997) 2313.

[28] S. Neumaier, G. Alkhazov, M. Andronenko, A. Dobrovolsky, P. Egelhof, G. Gavrilov, H. Geissel, H. Irnich, A. Khanzadeev, G. Korolev, A. Lobodenko, G. Münzenberg, M. Mutterer, W. Schwab, D. Seliverstov, T. Suzuki, N. Timofeev, A. Vorobyov, V. Yatsoura, Small-angle proton elastic scattering from the neutron-rich isotopes ^{6}He and ^{8}He, and from ^{4}He, at 0.7 GeV in inverse kinematics, Nucl. Phys. A 712 (2002) 247.

[29] G. Alkhazov, A. Dobrovolsky, P. Egelhof, H. Geissel, H. Irnich, A. Khanzadeev, G. Korolev, A. Lobodenko, G. Münzenberg, M. Mutterer, S. Neumaier, W. Schwab, D. Seliverstov, T. Suzuki, A. Vorobyov, Nuclear matter distributions in the ^{6}He and ^{8}He nuclei from differential cross sections for small-angle proton elastic scattering at intermediate energy, Nucl. Phys. A 712 (2002) 269.

[30] P. Egelhof, G. Alkhazov, M. Andronenko, A. Bauchet, A. Dobrovolsky, S. Fritz, G. Gavrilov, H. Geissel, C. Gross, A. Khanzadeev, G. Korolev, G. Kraus, A. Lobodenko, G. Münzenberg, M. Mutterer, S. Neumaier, T. Schäfer, C. Scheidenberger, D. Seliverstov, N. Timofeev, A. Vorobyov, V. Yatsoura, Nuclear-matter distributions of halo nuclei from elastic proton scattering in inverse kinematics, Eur. Phys. J. A 15 (2002) 27.
[31] A. Dobrovolsky, G. Alkhazov, M. Andronenko, A. Bauchet, P. Egelhof, S. Fritz, H. Geissel, C. Gross, A. Khanzadeev, G. Korolev, G. Kraus, A. Lobodenko, G. Münzenberg, M. Mutterer, S. Neumaier, T. Schäfer, C. Scheidenberger, D. Seliverstov, N. Timofeev, A. Vorobyov, V. Yatsoura, Study of the nuclear matter distribution in neutron-rich Li isotopes, Nucl. Phys. A 766 (2006) 1.
[32] S. Ilieva, F. Aksouh, G. Alkhazov, L. Chulkov, A. Dobrovolsky, P. Egelhof, H. Geissel, M. Gorska, A. Inglessi, R. Kanungo, A. Khanzadeev, O. Kiselev, G. Korolev, X. Le, Y. Litvinov, C. Nociforo, D. Seliverstov, L. Sergeev, H. Simon, V. Volkov, A. Vorobyov, H. Weick, V. Yatsoura, A. Zhdanov, Nuclear-matter density distribution in the neutron-rich nuclei ^{12,14}Be from proton elastic scattering in inverse kinematics, Nucl. Phys. A 875 (2012) 8.
[33] G. Korolev, A. Dobrovolsky, A. Inglessi, G. Alkhazov, P. Egelhof, A. Estradé, I. Dillmann, F. Farinon, H. Geissel, S. Ilieva, Y. Ke, A. Khanzadeev, O. Kiselev, J. Kurcewicz, X. Le, Y. Litvinov, G. Petrov, A. Prochazka, C. Scheidenberger, L. Sergeev, H. Simon, M. Takechi, S. Tang, V. Volkov, A. Vorobyov, H. Weick, V. Yatsoura, Halo structure of ^{8}B determined from intermediate energy proton elastic scattering in inverse kinematics, Phys. Letters B 780 (2018) 200.
[34] A. Dobrovolsky, G. Korolev, A. Inglessi, G. Alkhazov, G. Colò, I. Dillmann, P. Egelhof, A. Estradé, F. Farinon, H. Geissel, S. Ilieva, Y. Ke, A. Khanzadeev, O. Kiselev, J. Kurcewicz, X. Le, Y. Litvinov, G. Petrov, A. Prochazka, C. Scheidenberger, L. Sergeev, H. Simon, M. Takechi, S. Tang, V. Volkov, A. Vorobyov, H. Weick, V. Yatsoura, Nuclear-matter distribution in the proton-rich nuclei ^{7}Be and ^{8}B from intermediate energy proton elastic scattering in inverse kinematics, Nuclear Physics A 989 (2019) 40.
[35] A. Vorobyov, G. Korolev, V. Schegelsky, G. Solyakin, G. Sokolov, Y. Zalite, A method for studies of small-angle hadron-proton elastic scattering in the coulomb interference region, Nucl. Instr. Meth. 119 (1974) 509.
[36] H. Geissel, P. Armbruster, K. Behr, A. Brünle, K. Burkard, M. Chen, H. Folger, B. Franczak, H. Keller, O. Klepper, B. Langenbeck, F. Nickel, E. Pfeng, M. Pfützner, E. Roeckl, K. Rykaczewski, I. Schall, D. Schardt, C. Scheidenberger, K.-H. Schmidt, A. Schröter, T. Schwab, K. Sümmerer, M. Weber, G. Münzenberg, T. Brohm, H.-G. Clerc, M. Fauerbach, J.-J. Gaimard, A. Grewe, E. Hanelt, B. Knödler, M. Steiner, B. Voss, J. Weckenmann, C. Ziegler, A. Magel, H. Wollnik, J. Dufour, Y. Fujita, D. Vieira, B. Sherrill, The GSI projectile fragment separator (FRS): a versatile magnetic system for relativistic heavy ions, Nuclear Instruments and Methods in Physics Research Section B: Beam Interactions with Materials and Atoms 70 (1992) 286.
[37] J. Burq, M. Chemarin, M. Chevallier, A. Denisov, C. Doré, T. Ekelöf, P. Grafström, E. Hagberg, B. Ille, A. Kashchuk, G. Korolev, S. Kullander, M. Lambert, J. Martin, S. Maury, J. Paumier, M. Querrou, V. Schegelsky, E. Spiridenkov, I. Tkach, A. Vorobyov, Measurements of π^-p elastic scattering in the coulomb interference region at high energies, Phys. Lett. B 77 (1978) 438.
[38] A. Vorobyov, Y. Grigorev, Y. Zalite, G. Korolev, E. Maev, G. Sokolov, A. Khanzadeev, An ionization spectrometer for recoil nuclei in research on elastic small-angle scattering of hadrons, Instrum. Exp. Tech. 24 (1982) 1127.
[39] S. Lenzi, A. Vitturi, F. Zardi, Description of inelastic scattering between heavy ions in the Glauber model, Phys. Rev. C 38 (1988) 2086.
[40] C. Bertulani, C. Campbell, T. Glasmacher, A computer program for nuclear scattering at intermediate and high energies, Computer Physics Communications 152 (2003) 317.
[41] L. Tassie, A Model of Nuclear Shape Oscillations for γ-Transitions and Electron Excitation, Australian Journal of Physics 9 (1956) 407.
[42] URL `http://www.nndc.bnl.gov`.
[43] G. Colò, to be published .
[44] I. Angeli, K. Marinova, Table of experimental nuclear ground state charge radii: An update, Atomic Data and Nuclear Data Tables 99 (2013) 69.
[45] H. Fortune, Matter radii and configuration mixing in $^{15-19}$C, Eur. Phys. J. A 54 (2018) 73.
[46] B. Abu-Ibrahim, W. Horiuchi, A. Kohama, Y. Suzuki, Reaction cross sections of carbon isotopes incident on a proton, Phys. Rev. C 77 (2008) 034607.
[47] CODATA value: proton rms charge radius, URL `https://physics.nist.gov/cgi-bin/cuu/Value?rp`, 2018.
[48] Z. Ren, Z. Zhu, Y. Cai, G. Xu, Relativistic mean-field study of exotic carbon nuclei, Nuclear Physics A 605 (1996) 75.
[49] H. Sagawa, X. R. Zhou, X. Z. Zhang, T. Suzuki, Deformations and electromagnetic moments in carbon and neon isotopes, Phys. Rev. C 70 (2004) 054316.
[50] Y. Kanada-En'yo, Deformation of C isotopes, Phys. Rev. C 71 (2005) 014310.
[51] L. Grigorenko, B. Danilin, V. Efros, N. Shul'gina, M. Zhukov, Structure of the ^{8}Li and ^{8}B nuclei in an extended three-body model and astrophysical S_{17} factor, Phys. Rev. C 57 (1998) 2099(R).

Appendix

This Appendix contains in tabular form the measured cross sections $\mathrm{d}\sigma/\mathrm{d}t$ as a function of the four-momentum transfer squared $-t$ for p^{12}C and p^{14-17}C elastic scattering measured in the present experiment. Only statistical errors are indicated.

p^{12}C, E_{p}=705.2 MeV		p^{12}C, E_{p}=705.2 MeV	
$-t$, (GeV/c)^2	$\mathrm{d}\sigma/\mathrm{d}t$, mb/(GeV/$c$)^2	$-t$, (GeV/c)^2	$\mathrm{d}\sigma/\mathrm{d}t$, mb/(GeV/$c$)^2
0.00117	14965. ± 297.3	0.01300	2858.1 ± 67.1
0.00164	9489.3 ± 229.4	0.01490	2448.0 ± 60.5
0.00211	7942.5 ± 208.5	0.01694	2061.6 ± 54.3
0.00258	7060.1 ± 195.8	0.01910	1871.3 ± 50.7
0.00305	6335.2 ± 185.1	0.02140	1549.8 ± 45.3
0.00352	5742.1 ± 175.8	0.02382	1358.2 ± 41.7
0.00399	5620.2 ± 173.9	0.02636	1160.9 ± 38.0
0.00446	5290.9 ± 168.8	0.02904	924.7 ± 33.5
0.00493	5171.5 ± 166.9	0.03185	745.1 ± 29.8
0.00540	4517.4 ± 156.2	0.03478	589.2 ± 26.3
0.00586	4713.5 ± 159.9	0.03785	495.9 ± 24.0
0.00633	4636.6 ± 160.4	0.04104	383.7 ± 21.0
0.00680	4250.1 ± 155.3	0.04437	309.6 ± 18.9
0.00727	4317.7 ± 155.3	0.04782	223.6 ± 16.1
0.00774	3883.2 ± 147.3	0.05141	188.6 ± 14.9
0.00804	3793.6 ± 84.1	0.05513	131.3 ± 12.6
0.00956	3400.9 ± 77.7	0.05897	85.3 ± 10.4
0.01122	3023.1 ± 71.0		

p^{14}C, E_{p} = 704.4 MeV		p^{14}C, E_{p} = 704.4 MeV	
$-t$, (GeV/c)^2	$\mathrm{d}\sigma/\mathrm{d}t$, mb/(GeV/$c$)^2	$-t$, (GeV/c)^2	$\mathrm{d}\sigma/\mathrm{d}t$, mb/(GeV/$c$)^2
0.00117	16137. ± 435.8	0.00989	3859.5 ± 126.6
0.00164	10641. ± 322.6	0.01137	3242.1 ± 78.9
0.00211	8626.2 ± 284.4	0.01350	2855.9 ± 71.7
0.00258	7779.0 ± 254.7	0.01581	2434.2 ± 64.4
0.00305	7125.5 ± 245.8	0.01830	2024.8 ± 57.9
0.00352	6813.3 ± 241.4	0.02096	1686.9 ± 50.9
0.00399	6227.4 ± 228.9	0.02381	1434.8 ± 46.7
0.00446	5802.7 ± 223.0	0.02683	1131.7 ± 39.6
0.00493	5678.4 ± 218.2	0.03004	908.8 ± 35.3
0.00540	5115.2 ± 209.8	0.03342	705.7 ± 30.4
0.00586	4870.5 ± 211.9	0.03699	614.9 ± 28.6
0.00633	5206.6 ± 224.0	0.04074	413.7 ± 23.8
0.00680	5071.9 ± 218.3	0.04467	352.4 ± 23.0
0.00727	4894.1 ± 203.3	0.04878	253.5 ± 18.2
0.00774	4424.1 ± 180.1	0.05307	140.5 ± 14.6
0.00807	4368.8 ± 139.0	0.05755	133.9 ± 12.8
0.00896	4081.9 ± 132.7		

p^{15}C, $E_{\mathrm{p}} = 702.5$ MeV		p^{15}C, $E_{\mathrm{p}} = 702.5$ MeV	
$-t$, $(\mathrm{GeV}/c)^2$	$\mathrm{d}\sigma/\mathrm{d}t$, $\mathrm{mb}/(\mathrm{GeV}/c)^2$	$-t$, $(\mathrm{GeV}/c)^2$	$\mathrm{d}\sigma/\mathrm{d}t$, $\mathrm{mb}/(\mathrm{GeV}/c)^2$
0.00117	16475.9 ± 362.3	0.01069	3769.1 ± 89.2
0.00164	12658.6 ± 322.1	0.01290	3332.1 ± 80.9
0.00211	10386.9 ± 291.0	0.01532	2758.2 ± 71.2
0.00258	8961.4 ± 269.9	0.01793	2253.4 ± 62.6
0.00305	8421.4 ± 261.6	0.02075	1780.6 ± 54.2
0.00352	7541.3 ± 247.6	0.02377	1379.4 ± 46.7
0.00399	7553.8 ± 248.2	0.02699	1125.2 ± 41.3
0.00446	6746.6 ± 235.1	0.03042	850.1 ± 35.3
0.00493	6971.2 ± 239.6	0.03405	607.0 ± 29.4
0.00540	6003.9 ± 222.9	0.03789	410.5 ± 23.9
0.00586	6323.3 ± 229.7	0.04193	325.4 ± 21.0
0.00633	5916.3 ± 221.1	0.04617	206.0 ± 16.6
0.00680	5276.6 ± 208.6	0.05063	165.0 ± 14.7
0.00727	5385.0 ± 215.6	0.05529	94.3 ± 11.2
0.00774	4831.4 ± 206.5	0.06016	62.0 ± 9.1
0.00869	4818.7 ± 104.4		

p^{16}C, $E_{\mathrm{p}} = 700.5$ MeV		p^{16}C, $E_{\mathrm{p}} = 700.5$ MeV	
$-t$, $(\mathrm{GeV}/c)^2$	$\mathrm{d}\sigma/\mathrm{d}t$, $\mathrm{mb}/(\mathrm{GeV}/c)^2$	$-t$, $(\mathrm{GeV}/c)^2$	$\mathrm{d}\sigma/\mathrm{d}t$, $\mathrm{mb}/(\mathrm{GeV}/c)^2$
0.00117	19706.1 ± 495.4	0.01405	3295.4 ± 136.0
0.00164	12894.0 ± 412.0	0.01535	2828.7 ± 123.8
0.00211	11955.1 ± 394.6	0.01671	2488.2 ± 114.3
0.00258	9308.8 ± 346.6	0.01813	2115.6 ± 103.8
0.00305	9144.8 ± 343.3	0.01961	2099.7 ± 102.3
0.00352	8549.8 ± 331.8	0.02114	1863.2 ± 95.0
0.00399	7662.0 ± 314.4	0.02273	1496.5 ± 84.1
0.00446	7337.3 ± 307.9	0.02438	1368.8 ± 79.5
0.00493	7317.3 ± 308.0	0.02609	1133.0 ± 71.5
0.00540	6907.9 ± 300.3	0.02785	922.9 ± 63.9
0.00586	6707.5 ± 296.5	0.02967	856.7 ± 61.1
0.00633	5881.3 ± 276.2	0.03155	729.5 ± 55.8
0.00680	6069.1 ± 277.1	0.03349	592.8 ± 49.9
0.00727	5263.5 ± 265.4	0.03548	507.3 ± 45.9
0.00774	5162.7 ± 266.9	0.03858	374.0 ± 27.7
0.00838	5235.1 ± 188.7	0.04291	304.7 ± 24.7
0.00940	4564.0 ± 173.9	0.04748	178.3 ± 18.9
0.01047	4302.8 ± 165.1	0.05228	115.4 ± 15.1
0.01161	3954.3 ± 154.7	0.05732	63.6 ± 11.5
0.01280	3543.2 ± 143.6		

p^{17}C, $E_{\mathrm{p}} = 703.2$ MeV		p^{17}C, $E_{\mathrm{p}} = 703.2$ MeV	
$-t$, $(\mathrm{GeV}/c)^2$	$\mathrm{d}\sigma/\mathrm{d}t$, $\mathrm{mb}/(\mathrm{GeV}/c)^2$	$-t$, $(\mathrm{GeV}/c)^2$	$\mathrm{d}\sigma/\mathrm{d}t$, $\mathrm{mb}/(\mathrm{GeV}/c)^2$
0.00117	18437.1 ± 429.9	0.01460	3160.4 ± 108.3
0.00164	13783.9 ± 361.8	0.01601	2718.3 ± 98.8
0.00211	12008.3 ± 335.5	0.01748	2508.4 ± 93.5
0.00258	10474.2 ± 312.1	0.01901	2210.0 ± 86.5
0.00305	9801.4 ± 301.2	0.02062	1830.3 ± 77.8
0.00352	9018.8 ± 288.7	0.02228	1758.0 ± 75.4
0.00399	9179.1 ± 291.5	0.02401	1443.9 ± 67.6
0.00446	8061.6 ± 273.2	0.02581	1200.3 ± 61.1
0.00493	7765.3 ± 268.8	0.02766	1007.4 ± 55.6
0.00540	7172.2 ± 258.9	0.02959	892.8 ± 51.9
0.00586	7054.6 ± 257.8	0.03158	689.5 ± 45.5
0.00633	7343.3 ± 266.4	0.03363	543.5 ± 40.2
0.00680	6387.0 ± 252.1	0.03575	461.0 ± 37.0
0.00727	6230.8 ± 245.6	0.03794	394.7 ± 34.1
0.00774	5526.5 ± 231.5	0.04019	285.1 ± 29.1
0.00853	5705.9 ± 160.4	0.04369	210.8 ± 17.7
0.00961	4955.8 ± 147.2	0.04858	125.0 ± 13.8
0.01076	4738.9 ± 140.7	0.05374	62.9 ± 10.1
0.01198	3829.4 ± 123.7	0.05916	44.4 ± 8.5
0.01326	3681.4 ± 119.0		